JOURNAL OF CATALYSIS 150, 34–45 (1994)

Selective Conversion of *n*-Butene to Isobutylene at Extremely High Space Velocities on ZSM-23 Zeolites

Wen-Qing Xu,* Yuan-Gen Yin,* Steven L. Suib,*,†,‡,[1] and Chi-Lin O'Young§,[1]

*U-60, Department of Chemistry, University of Connecticut, Storrs, Connecticut 06269-3060; †Department of Chemical Engineering, University of Connecticut, Storrs, Connecticut 06269; ‡Institute of Materials Science, University of Connecticut, Storrs, Connecticut 06269; and §Texaco, Inc., Research and Development Center, P. O. Box 509, Beacon, New York 12508

Received April 20, 1994; revised June 27, 1994

n-Butene has been isomerized to isobutylene on zeolite ZSM-23 catalysts at extremely high space velocities from 171 to 342 WHSV. The zeolite catalysts were prepared with hydrothermal methods by using pyrrolidine as a structure-directing template. The prepared materials have been characterized by SEM-EDX, XRD, FTIR, AA-ICP, TPD, BET surface area/pore size distributions, and pyridine chemisorption. Selectivities to isobutylene ranged from 85 to 95% and yields of isobutylene from 30 to 20%, depending on the space velocity of but-1-ene. Good stability in the catalytic activity for *n*-butene skeletal isomerization is an important characteristic of such ZSM-23 zeolites. Isobutylene is believed to be formed from *n*-butene via a methyl cyclopropane carbenium intermediate and this is a reversible process. Dimerization of butene molecules is a primary side reaction for *n*-butene skeletal isomerization. The dimerized products (octenes) are further cracked into propylene and pentenes via β-scission of carbenium intermediates. Propylene, a product of the secondary reaction, is then dimerized to form hexenes or codimerized with butene to form heptenes. Conversion of but-1-ene to *cis*/*trans*-but-2-enes is greater than one predicts from thermodynamic equilibrium data. *cis*-But-2-ene is observed to be the preferential product for but-1-ene double bond migration. The preferential formation of *cis*-but-2-ene is due to a steric interaction of the methyl group in the secondary butyl carbenium intermediate with the pore wall of the small pore zeolite, ZSM-23. Zeolite ZSM-23 also shows shape selectivity for adsorption of ammonia, but-1-ene, and isobutylene. The shape selectivities of these materials are further improved after aging of catalysts used in but-1-ene skeletal isomerization.

INTRODUCTION

Oxygenated species are now the major boosters of octane number since new EPA regulations have limited the content of aromatics and olefins in gasoline. MTBE (methyl *t*-butyl ether) is currently used to improve octane number although other oxygenated species have been proposed (1). However, the source of isobutylene for the production of MTBE is greatly limited by the supply from the catalytic cracking of petroleum. Therefore, finding a new isobutylene source via *n*-butene skeletal isomerization is of great practical significance.

Szabo *et al.* (2) and Choudhary (3) reported using fluorinated γ-alumina as a catalyst for this isomerization with limited success. Results of such studies imply that both suitable acidity and pore size for zeolite catalysts may be necessary to achieve desirable activity and selectivity to isobutylene. Zeolite Y contains supercages of 13 Å in diameter with 12-member ring openings (7.4 Å) in which coke is rapidly formed. Hence, Zeolite Y is rapidly deactivated by such coke (after several seconds) (4).

Thomas has predicted that 10-member ring zeolites may have the ability to selectively isomerize *n*-butene to isobutylene (5). ZSM-5, a 10-member ring medium-pore zeolite (5.3 × 5.6, 5.1 × 5.5 Å), is a coke-resistant catalyst in the presence of olefins. For example, it is used as a catalyst for interconversion of olefins (6). However, the selectivity to isobutylene in butene isomerization for this zeolite is low partly because the strong acidity of ZSM-5 catalyzes side reactions, such as butene dimerization followed by cracking to light hydrocarbons.

In our previous work (7–10), substitution of aluminum with boron in ZSM-5 and ZSM-11 leads to a reduced acid strength, resulting in a suppression of dimerization and cracking and an improvement in selectivity to isobutylene. Further suppression of butene dimerization has been found to be limited for boron-substituted ZSM-5 and ZSM-11 due to their medium-size pores and relatively large channel intersections (about 9 Å in diameter) (7, 9, 10). The pore sizes of ZSM-5 and ZSM-11 are large enough to accommodate octenes so that butene dimerization cannot be prohibited.

Recently, two patents suggest that ferrierite/ZSM-35, a 10-member ring small pore zeolite, is a good catalyst for butene isomerization (11, 12). Ferrierite/ZSM-35 has an orthorhombic framework containing one-dimensional channels of 10-member rings (4.2 × 5.4 Å) and one-dimen-

[1] To whom correspondence should be addressed.

0021-9517/94 $6.00

sional channels of 8-member rings (3.5 × 4.8 Å). These two kinds of channels are perpendicularly intersected. The 8-member ring channels contain spherical cavities with a size of about 6 to 7 Å.

Our previous work (13) showed that the yield and selectivity to isobutylene for *n*-butene isomerization on ferrierite/ZSM-35 are both increased with time on stream. Side reactions for *n*-butene isomerization are mainly controlled by two factors, i.e., acidity and limitations of pore size. Poisoning of strong acid sites by coke deposition leads to suppression of dimerization reactions. The deposited coke is aromatic in nature and its hydrogen to carbon ratio decreases with time on stream. Coke deposition also blocks channels and modifies the space around acid sites so that acid sites do not have enough space for dimerization reactions (13). Such blocking produces significant contributions for shape selectivity for skeletal isomerization of *n*-butene. In addition, kinetic studies of coke formation lead to a conclusion that the coke formation is limited by the micropore volume of ferrierite/ZSM-35.

ZSM-23 zeolite has an orthorhombic framework structure containing one-dimensional channels of 10-member rings (4.5 × 5.2 Å) (14). As compared to ferrierite/ZSM-35 having cavities of about 6–7 Å, ZSM-23 may have unique coke resistant and antideactivation properties for *n*-butene isomerization to isobutylene.

In this work, ZSM-23 zeolites have been successfully prepared and *n*-butene skeletal isomerization over such ZSM-23 zeolites has been intensively investigated. Good selectivities (95%) and yields (28%) have been achieved for *n*-butene skeletal isomerization to isobutylene over ZSM-23 zeolites. Space velocities of but-1-ene range from 171 to 342 WHSV. Such large space velocities would lead to a 32 to 64 times smaller reactor, as compared to ferrierite/ZSM-35 catalysts having a but-1-ene space velocity of 5.34 WHSV. ZSM-23 zeolites also show very good stability in yields and selectivities to isobutylene at such high space velocities. The operation span for but-1-ene space velocities (from 171 to 342 WHSV) may allow the commercialization of ZSM-23 zeolite catalyst systems. The mechanism for *n*-butene skeletal isomerization and its relevant side reactions are also discussed. Adsorptions of ammonia, but-1-ene, and isobutylene on ZSM-23 zeolites have been studied in order to elucidate shape selective characteristics of such zeolite catalysts.

EXPERIMENTAL SECTION

A. Synthesis of ZSM-23

ZSM-23 zeolites were prepared with hydrothermal methods by using pyrrolidine as a structure-directing template. The precursor gel contained 110 parts of SiO_2, 1 part of Al_2O_3, 4.24 parts of Na_2O, 70.2 parts of pyrrolidine, and 2200 parts of H_2O. In most experiments, 16.85 g of 1-*M* NaOH, 1.971 g of NaCl, and 1.269 g of $NaAlO_2$ were added into a beaker containing 171.0 g of water. The resultant aqueous solution was then mixed with 35.88 g of pyrrolidine. About 170.3 g of Ludox HS-40 were added into the above solution while stirring to form a gel. The gel was divided into five stainless steel autoclaves with Teflon liners of 110 ml volume. These autoclaves were then put into an oven in which temperature was controlled at 448 K. Hydrothermal reactions were terminated by taking these five autoclaves out of the oven after 20, 40, 60, 80, and 100 hr, respectively. Resultant solid powders were then filtered, washed with DDW, and dried at 403 K overnight to obtain NaZSM-23 zeolites. These materials were then calcined at 823 K for 4 hr in nitrogen and another 4 hr in air. NH_4ZSM-23 zeolites were obtained by ion-exchange of their alkali forms two times with 1 *M* aqueous solution of ammonium nitrate at 353 K. These zeolites were analyzed by ICP methods.

B. Characterization

X-ray diffraction (XRD) experiments were done on a Scintag Model XDS 2000 diffractometer with a monochromatic X-ray beam and scintillator. Samples were mounted on a glass plate that remained horizontal during all experiments. A beam voltage of 45 kV and a current of 40 mA were used with Cu $K\alpha$ radiation.

Scanning electron microscopy (SEM) and energy dispersive X-ray (EDX) analyses were done on an Amray Model 1810 D microscope with an Amray PV 9800 energy dispersive X-ray analyzer. This energy dispersive X-ray analyzer was equipped with a windowless detector for observation of elements with atomic numbers smaller than Na and greater than Be.

Fourier transform infrared (FTIR) experiments were done on a Nicolet 750 spectrometer at a resolution of 4 cm^{-1} by using either KBr pellets or self-supporting wafers. Pyridine chemisorption experiments were done on self-supported wafers in an *in situ* IR cell. The sample was dehydrated at 823 K for 5 hr under a vacuum of 10^{-5} Torr followed by adsorption of purified pyridine vapor at room temperature for 15 min. Then the system was evacuated at 432 K overnight to remove physisorbed pyridine and an infrared spectrum was then recorded.

Pore size distributions were determined by nitrogen adsorption and desorption data acquired on an Omicron Omnisorp 100CX adsorptive and desorptive apparatus. The sample was pretreated overnight at 723 K under a vacuum of 10^{-6} Torr. The Kelvin theory was used to determine the distributions of meso- and macro-pores. The Horvath–Kawazoe method (15) was used to determine the distribution of micropores.

Temperature-programmed desorption (TPD) experiments were done on a TPD apparatus described pre-

viously (7, 16). The sample was first heated from room temperature to 823 K at a ramping rate of 15 K/min and then soaked at 823 K for 1 hr under a flow of 30 ml/min ultrapure helium. The system was then cooled to 373 K over 100 min. Adsorbates (ammonia, but-1-ene, or isobutylene) were then flowed over the sample for 30 min. The sample was then purged with helium for 40 min in order to eliminate physisorbed species. The temperature was ramped at 15 K/min from 373 to 883 K and TPD data were acquired.

C. Catalysis

Butene isomerization reactions were carried out in a microreactor loaded with different amounts of zeolite catalysts at a pressure of one atmosphere. The reactor was heated from room temperature to 823 K at a ramping rate of 15 K/min in a flow of nitrogen of 60 ml/min. The temperature of the reactor was maintained at 823 K for 30 min. Then the reactor was cooled to 693 K for 20 min. The reactor was then maintained at 693 K and the nitrogen flow was switched to a mixture of but-1-ene and nitrogen (1 : 1 molar ratio). Flow rates of both but-1-ene and nitrogen were controlled for different space velocities. Reaction products were analyzed every hour after 10 min on stream with a Hewlett Packard 5890 Series II GC. This GC was equipped with a GS-Alumina capillary column (J & W Scientific) and a thermal conductivity detector (TCD). Literature values for TCD response coefficients were used for calibration (17, 18).

RESULTS

A. Morphology-SEM

Autoclave of the precursor gel for 20 hr did not produce ZSM-23 crystals, which was confirmed by SEM and XRD studies. ZSM-23 crystals were initially observed in the sample which was autoclaved for 40 hr, Fig. 1a. They have rice-like morphology (about 6 μ) in length and 3 μm in width). However, Fig. 1a also shows some aggregated particles. Such aggregated particles are amorphous materials and disappear gradually with autoclave time (60, 80, and 100 hr), as shown by SEM results in Fig. 1b–1d, respectively. The sample treated in the autoclave for 100 hr has a silicon to aluminum ratio of 59.7 which was determined by ICP methods.

B. Structure-XRD

The structure of ZSM-23 for these prepared samples was confirmed by XRD results. Figure 2 shows typical XRD patterns for the sample treated in an autoclave for 100 hr, which is consistent with all XRD lines of ZSM-23 zeolites. Figure 3 shows a correlation of the diffraction line intensity at d = 4.052 Å with autoclave time. The longer the precursor gel was autoclaved, the stronger the diffraction intensity at a line of d = 4.052 Å.

The pH of the mother liquor of these systems was also monitored and it is plotted versus different autoclave times in Fig. 4. A minimum pH was observed for the sample which was autoclaved for 20 hr at which there was no formation of ZSM-23 crystals. As ZSM-23 crystals formed, the pH was then increased up to 12.6.

C. BET Surface Area and Pore Size Distributions

Zeolite samples were calcined in two steps, i.e., at 823 K for 4 hr in nitrogen and another 4 hr in air. The objectives of the two step calcination were to thermally decompose organic templates in an inert atmosphere (nitrogen) and then to burn the decomposition residues off by oxygen (air). This avoided occurrence of a steaming atmosphere during zeolite calcination since direct introduction of air into the system would combust organic templates to form a significant amount of steam. Sodium ions in these calcined ZSM-23 zeolites were then ion-exchanged two times with a 1-*M* aqueous solution of ammonium nitrate at 353 K. The resultant ZSM-23 zeolites of ammonium form were then used for BET surface areas/pore size distributions, FTIR, acidity, and catalysis studies. ZSM-23 zeolites of hydrogen forms were usually *in situ* generated from their ammonium forms.

Table 1 shows data of BET surface areas and pore size distributions of meso- and macropores for ZSM-23 zeolites which were autoclaved for 40 and 100 hr, respectively. ZSM-23 zeolite autoclaved for 100 hr has more macropores (>100 Å) than samples autoclaved for 40 hr. However, meso- (10-100Å) and micro- (<10 Å) pore volumes for ZSM-23 zeolite autoclaved for 100 hr are less than those for ZSM-23 zeolite autoclaved for 40 hr. Therefore, surface areas of both meso-/macro- and micropores for ZSM-23 zeolite autoclaved for 40 hr are greater than those for ZSM-23 zeolite autoclaved for 100 hr.

After ZSM-23 zeolite (autoclaved for 100 hr) was used for catalytic reactions for 20 hr at 693 K, its meso-/macropore volumes were not changed significantly (Table 1). However, the micropore volume was drastically reduced from 58.4 μl/g (fresh) to 11.0 μl/g (used) due to coke formation. Therefore, the total surface area for this ZSM-23 zeolite was decreased from 275.3 m^2/g (fresh) to 210 m^2/g (used). Such a decrease in the surface area is mainly due to micropore blocking (from 77.2 m^2/g to 16.9 m2/g).

Figure 5 illustrates micropore distributions for the above three samples. There is a sharp distribution of micropores at 5.7 Å for ZSM-23 zeolite autoclaved for 40 hr, Fig. 5a. As compared to ZSM-23 zeolite autoclaved for 40 hr, ZSM-23 zeolite autoclaved for 100 hr has less micropore volume (Fig. 5b). Meanwhile, the maximum of the micropore distributions is shifted from 5.7 to 5.2

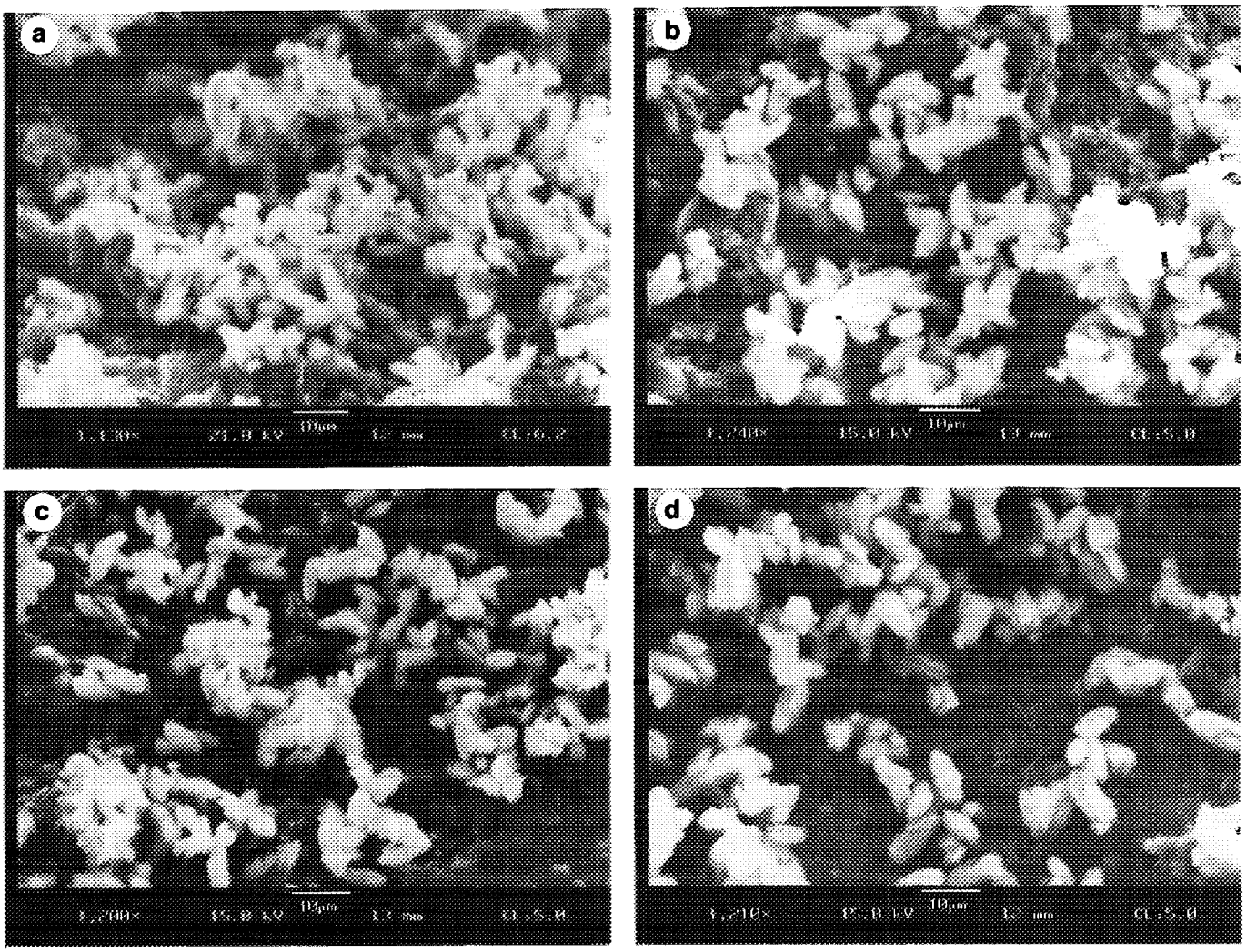

FIG. 1. Scanning electron microscopic data for monitoring zeolite ZSM-23 synthesis at different autoclave times: (a) 40 hr, (b) 60 hr, (c) 80 hr, and (d) 100 hr.

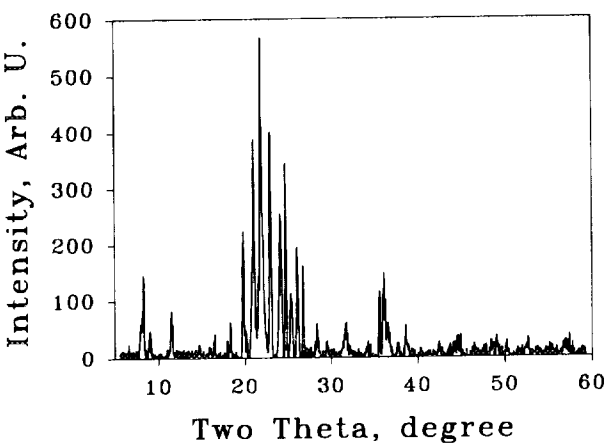

FIG. 2. Typical X-ray diffraction patterns for ZSM-23 zeolites (autoclaved for 100 hr).

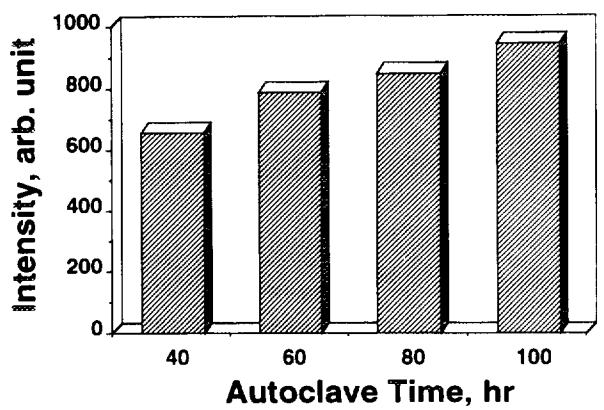

FIG. 3. Correlation of the diffraction intensity at *d* spacing of 4.052 Å with autoclave time.

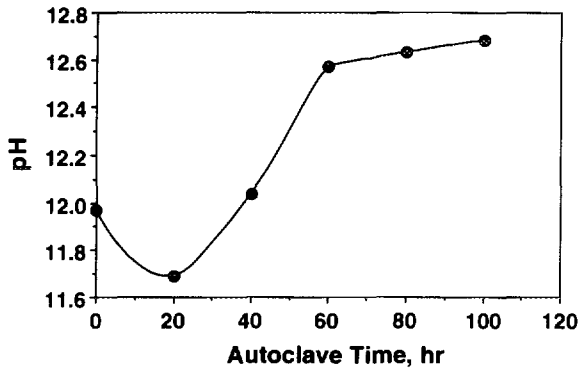

FIG. 4. The pH of mother liquors after different autoclave times.

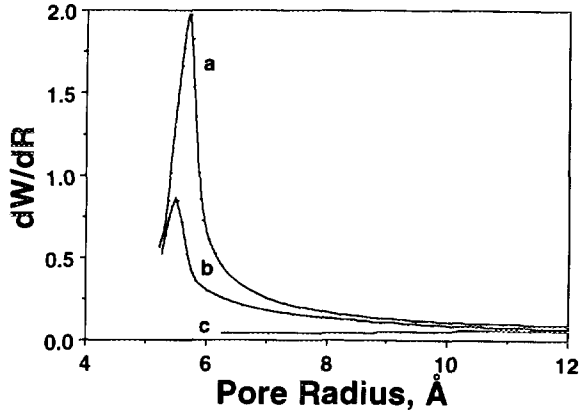

FIG. 5. Micropore size distributions of ZSM-23 zeolites: (a) autoclaved for 40 hr, (b) autoclaved for 100 hr, and (c) (b) used in *n*-butene skeletal isomerization at 693 K for 20 hr.

Å for ZSM-23 zeolites autoclaved for 40 to 100 hr, respectively. The used catalyst (ZSM-23 zeolite autoclaved for 100 hr) loses most micropore volume due to coke formation (Fig. 5c).

D. Acidity-FTIR

FT-IR spectra for ZSM-23 zeolites of different autoclave times are shown in Fig. 6a (40 hr) and Fig. 6c (100 hr). Since these FT-IR spectra were acquired on self-supported wafers (about 10 mg), IR radiation of about 1100, 800, and below 500 cm^{-1} was completely absorbed. However, self-supported wafers allow observation of weak IR bands of the studied materials. For example, weak IR bands of ZSM-23 zeolites are clearly observed at 3744 cm^{-1} (hydroxyl group of terminal silanol), 3609 cm^{-1} (hydroxyl group of acid sites, associated with framework silicon and aluminum ions), 1982, 1877, 1628, and 646 cm^{-1}. The ratio of the IR band at 3744 cm^{-1} to that at 3609 cm^{-1} for ZSM-23 zeolite autoclaved for 40 hr (4.25) is greater than that for ZSM-23 zeolite autoclaved for 100 hr (0.92).

Chemisorption of pyridine was also studied on ZSM-23 zeolites which were autoclaved for different times (Fig. 6b and Fig. 6d). ZSM-23 zeolites have both Brønsted (1540 cm^{-1}) and Lewis acid sites (1460 cm^{-1}). There are no significant differences in Brønsted acid sites between ZSM-23 zeolites autoclaved for 40 hr (Fig. 6b) and for 100 hr (Fig. 6d). However, the ratio of Brønsted to Lewis acid sites for ZSM-23 zeolite autoclaved for 100 hr (7.58) is much greater than that for 40 hr (1.50).

E. Acidity-TPD

Figure 7 shows ammonia TPD data for ZSM-23 zeolites. Two desorption peaks are observed at 448 and 663 K for

TABLE 1

Pore Size Distributions of Fresh and Used ZSM-23 Zeolites

Pore radius (Å)	Pore volume (μl/g)		
	A[a]	B[b]	C[c]
300–200	42.9	126.0	136.0
200–100	91.9	165.0	141.0
100–50	95.5	55.4	53.0
50–40	39.0	22.2	21.7
40–30	57.7	36.3	35.4
30–20	92.2	69.7	68.5
20–10	137.0	92.7	90.4
Meso, Macropore (>10 Å)	556.0	568.0	545.0
Micropore (<10 Å)	69.2	58.4	11.0
Surface area (total), m^2/g	392.7	275.3	210.0
Surface area (>10 Å), m^2/g	277.8	198.1	193.1

[a] A, autoclaved for 40 hr.
[b] B, autoclaved for 100 hr.
[c] C, B used in *n*-butene skeletal isomerization at 693 K for 20 hr.

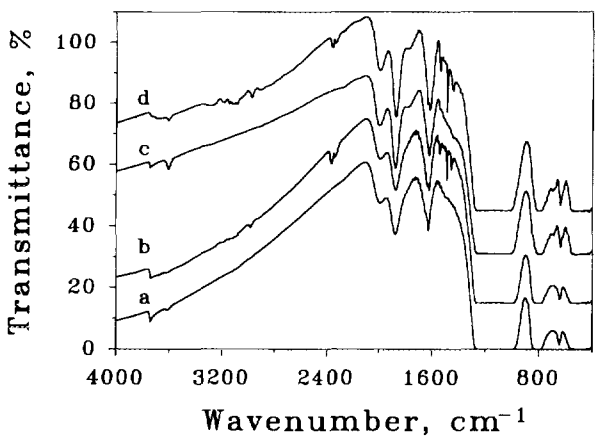

FIG. 6. FT-IR spectra of self-supported wafers of ZSM-23 zeolites: (a) autoclaved for 40 hr, (b) pyridine-chemisorbed (a), (c) autoclaved for 100 hr, and (d) pyridine-chemisorbed (c).

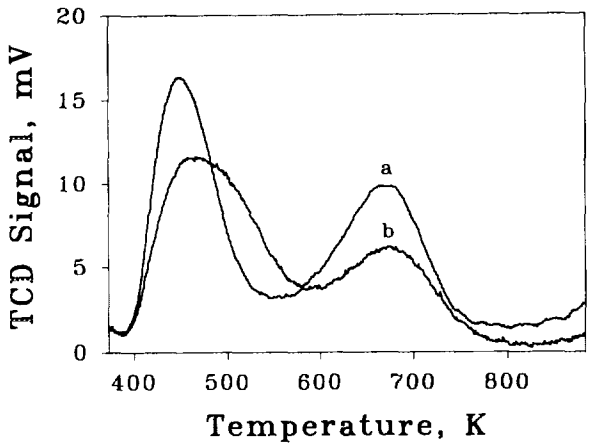

FIG. 7. Results of temperature-programmed desorption of ammonia over ZSM-23 zeolites: (a) fresh (b) used.

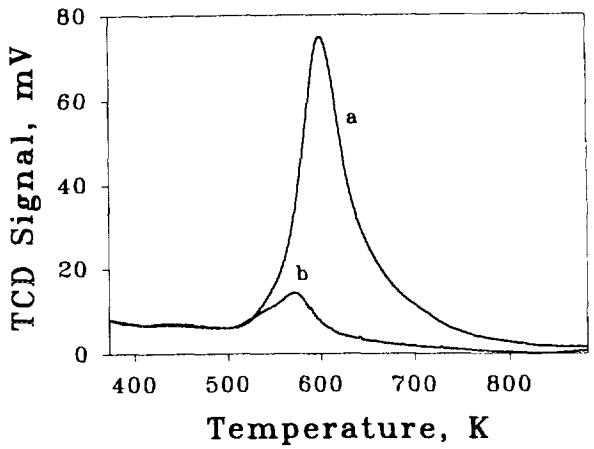

FIG. 8. Results of temperature-programmed desorption of *but*-1-ene over ZSM-23 zeolites: (a) fresh (b) used.

the fresh sample. The total amount of desorbed ammonia is 0.455 NH_3 per unit cell ($(NH_4)_nAl_nSi_{24-n}O_{48}$ is defined as a unit cell of ZSM-23). The amount of Brønsted acid sites is estimated to be 0.402 protons per unit cell via the ratio of Brønsted to Lewis acid sites, i.e., 0.455x(7.58/8.58). Therefore, the ratio of silicon to framework aluminum is estimated to be 58.7 which is consistent with the result from ICP analyses (Si/Al = 59.7). In addition, the ratio of the amount of acid sites under the peak at 448 K to that at 663 K is 1.22.

For the used catalyst, the amount of acid sites under the low temperature peak (448 K) is the same as that for the fresh one except the peak is broadened. However, the amount of acid sites under the high temperature peak is decreased from 0.205/u.c. to 0.133/u.c.

F. Adsorption of But-1-ene and Isobutylene

But-1-ene TPD of ZSM-23 shows one desorption peak at 598 K (Fig. 8). For the fresh sample, the uptake of but-1-ene (0.476/u.c.) is similar to that of ammonia (0.455/u.c.). The uptake of but-1-ene for the used sample is 0.062/u.c. (about 13% of that of the fresh sample) and the desorption peak shifted to a lower temperature (570 K). Some but-1-ene molecules are converted to its isomers (*cis*-but-2-ene, *trans*-but-2-ene, and isobutylene) during temperature-programmed desorption.

TPD data for isobutylene show two desorption peaks at 475 and 573 K (Fig. 9). The uptake for isobutylene, 0.192/u.c., for the fresh sample is much less than that for ammonia (0.455/u.c.). The used catalyst also has two desorption peaks at the same temperatures as those of the fresh catalyst. However, the used sample only has 0.065 adsorbed isobutylene molecules per unit cell which is similar to that for but-1-ene (0.062/u.c.). The ratio of isobutylene uptake at low temperature to that at high temperature is about 0.55 for both fresh and used samples. Some isobutylene molecules can also be converted to its isomers, *n*-butenes, during temperature-programmed desorption.

G. Catalysis

But-1-ene space velocity. Our previous work showed that catalytic reactions of *n*-butene isomerization to isobutylene were carried out over ferrierite/ZSM-35 zeolites at 693 K with a typical but-1-ene space velocity of 5.34 WHSV (13). Similar conditions were also used to study catalytic properties of ZSM-23 zeolites. Reaction products were monitored by GC analysis every hour from 10 min to 20 hr time on stream. Results showed that ZSM-23 zeolites had very stable activities and selectivities with time on stream. Therefore, their average values for 20-hr

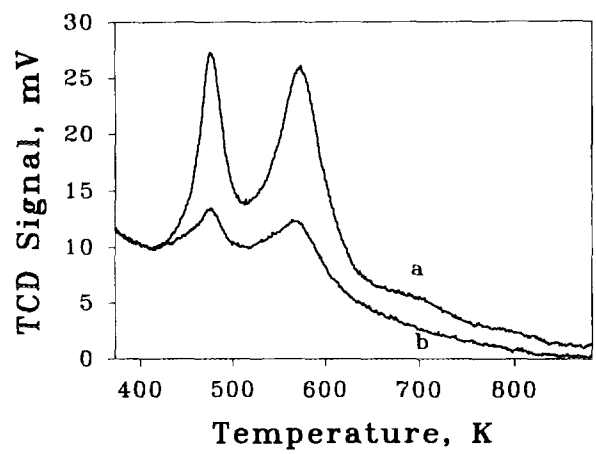

FIG. 9. Results of temperature-programmed desorption of isobutylene over ZSM-23 zeolites: (a) fresh (b) used.

TABLE 2

Product Distributions for Butene Skeletal Isomerization on Zeolite ZSM-23 at Different Temperatures and Space Velocities[a]

Feed	n-C_4^{2-}					i-C_4^{2-}	n-C_4^{2-}
WHSV	5.34	10.68	21.36	42.72	85.44	85.44	85.44
(T, K)	693	693	693	693	693	693	653
C_2^{2-}	1.01	0.46	0.24	0.11	0.07	0.03	0.02
C_3^{2-}	2.39	1.00	0.57	0.23	0.13	0.08	0.13
C_3^{2-}	14.28	11.27	8.87	5.48	3.92	3.26	2.88
iC_4	4.02	2.33	1.52	0.75	0.48	0.59	0.41
C_4	2.68	1.94	1.44	0.98	0.77	0.18	0.81
t-C_4^{2-}	8.47	12.30	15.71	20.75	24.59	13.99	27.58
l-C_4^{2-}	4.94	7.08	7.21	9.83	12.29	7.76	13.46
i-C_4^{2-}	17.17	24.61	30.25	31.91	29.13	52.89	21.61
c-C_4^{2-}	5.85	8.94	11.33	14.99	17.95	10.63	19.60
C_5^{2-}	18.62	15.58	12.31	7.32	5.03	4.82	4.08
C_6^{2-}	10.46	6.14	3.50	1.29	0.55	0.56	0.65
C_7^{2-}	6.94	5.82	4.05	2.22	1.07	1.31	1.68
C_8^{2-}	3.16	2.53	3.00	4.18	4.02	3.92	7.11
$S(i\text{-}C_4^{2-})$	21.37	34.34	46.08	58.73	64.65	68.89[b]	54.95
$X(n\text{-}C_4^{2-})$	80.74	71.68	65.75	54.43	45.17	47.11[c]	39.36

[a] Percent yield of products is defined in the text, Eq. [1]; Data are reported as the average values of 20 hr time on stream.
[b] Selectivity to n-butenes.
[c] Conversion of isobutylene.

analyses are tabulated in Table 2. The conversions are calculated on the basis that the three n-butene isomers are considered as reactants. The yields of all products are defined as

$$\%\ \text{Yield of } C_i = \frac{(\text{Moles of Produced } C_i) \times i}{(\text{Moles of } 1 - C_4^{2-}\ \text{Feed}) \times 4}. \quad [1]$$

Very high conversions (80.74%) and very low selectivities to isobutylene (21.37%) were obtained for ZSM-23 zeolites under such reaction conditions. The yield of isobutylene (17.17%) is far from its thermodynamic value (40.4%) at this temperature. Large amounts of heavier olefins were formed in addition to n-butene skeletal isomerization, i.e., 18.62% of pentenes, 10.46% of hexenes, 6.94% of hexenes, and 3.16% of octenes. No olefins which have more than eight carbons were observed. Besides propylene (14.28%), side products also include significant amounts of light alkanes, i.e., propane (2.39%), isobutane (4.02%), and n-butane (2.68%).

The space velocity of but-1-ene was then increased to 5.34×2^n WHSV ($n = 0$ to 4). Accordingly, the selectivity to isobutylene was increased from 21.37 to 64.65% and conversion of n-butene was decreased from 80.74 to 45.17%. The yield to isobutylene was maximized (31.9%) at a space velocity of 42.72 WHSV, 31.91%. Concentrations of all side products except octenes decreased as the space velocity of but-1-ene increased. Decreasing trends for these side products with WHSV are very different. These different trends will be discussed in more detail in order to elucidate the reaction mechanism.

Reaction temperature. The reaction temperature was decreased from 693 to 653 K at the but-1-ene space velocity of 85.44 WHSV. Such change led to a decrease in the yield of isobutylene from 29.13 to 21.61%. However, the total concentration of side products was increased from 16.04 to 17.75%. Hence, the selectivity to isobutylene was accordingly decreased from 64.65 to 54.95%. In addition, it is interesting that the formation of octenes, heptenes, and hexenes at the lower reaction temperature were increased as compared to those at the higher reaction temperature, while the formation of propylene and pentenes were decreased.

Optimization of conversion and selectivity. The above results suggest that increasing both the space velocity of but-1-ene and reaction temperature would be a solution for achieving highly selective conversion of n-butene to isobutylene. The reaction temperature was increased from 693 to 733 K and the space velocity of but-1-ene from 85.44 to 170.88 WHSV. Activities for butene isomerization on ZSM-23 were also very stable, as shown in Fig. 10. The initial selectivity to isobutylene (10 min on stream) was as high as 72.18%. Then the selectivity to isobutylene was slowly increased from 80.30 to 87.77% from 70 to 1150 min time on stream. The average selectiv-

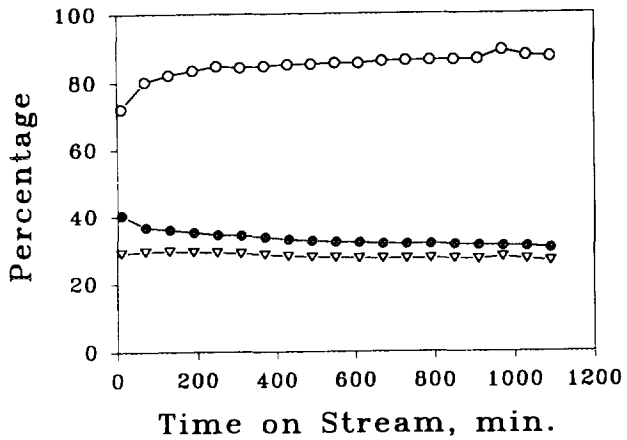

FIG. 10. *n*-Butene isomerization to isobutylene over zeolite ZSM-23 at 733 K with a *but*-1-ene space velocity of 170.88 WHSV. (open circle, selectivity to isobutylene; solid circle, conversion of *n*-butene; and open reciprocal triangle, yield of isobutylene).

ity to isobutylene in 20 hr on stream was as high as 84.80%. The yield of isobutylene changed from 29.18 to 27.21% and the average yield after 20 hr on stream was 28.17%. Side products for *n*-butene skeletal isomerization under such conditions are propylene (1.76%), pentenes (1.91%), and octenes (0.72%). Figure 11 presents results of *n*-butene isomerization at 737 K with an even higher space velocity of but-1-ene, 341.76 WHSV. At such an extremely high WHSV, butene skeletal isomerization was also successfully carried out. The yield of isobutylene was still maintained at 19.85% and the selectivity to isobutylene was further improved to 91.93% (an average value after 20 hr time on stream). Only small amounts of propylene (0.77%) and pentenes (0.74%) were observed as side products.

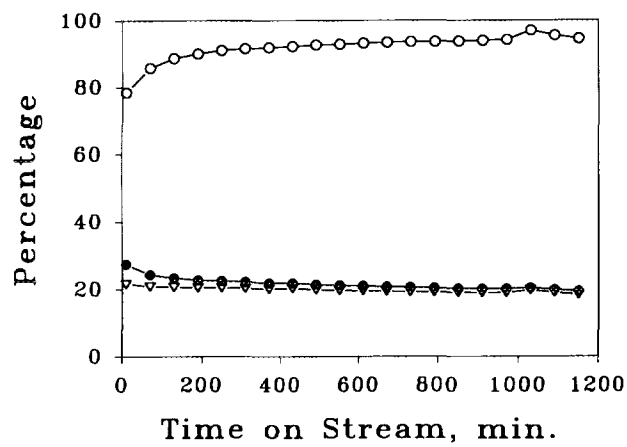

FIG. 11. *n*-Butene isomerization to isobutylene over zeolite ZSM-23 at 733 K with a *but*-1-ene space velocity of 341.76 WHSV. (open circle, selectivity to isobutylene; solid circle, conversion of *n*-butene; and open reciprocal triangle, yield of isobutylene).

Isobutylene as a feed. Isobutylene was also used as a feed for the catalyst of ZSM-23 zeolites at 693 K with a space velocity of 85.44 WHSV. Average values of catalytic properties for samples treated for 20 hr are also listed in Table 2. Isobutylene (47.11% in the feed) was converted to *n*-butene isomers (32.37%) and side products. Distributions of side products for using isobutylene as a feed were actually very similar to those for using but-1-ene as a feed, except that the ratio of *n*-butane to isobutane was entirely different for these two different feeds.

DISCUSSION

A. Synthesis and Characterization

ZSM-23 zeolites have been successfully synthesized with hydrothermal methods by using pyrrolidine as a structure-directing template. SEM results (Fig. 1) show that ZSM-23 zeolites have rice-like morphologies, consistent with literature results (19). ^{13}C CPMAS NMR spectroscopic studies were done by Kumar *et al.* (20) to study interactions of template molecules and the framework of ZSM-23 zeolites. It was revealed that pyrrolidine molecules are occluded as neutral, chemically intact species in the unidimensional, nonintersecting 10-member ring channels of ZSM-23 zeolites. In addition, Kumar *et al.* (21) also isomorphously substituted iron into the framework of zeolite ZSM-23 with pyrrolidine as a structure-directing template.

There is a minimum pH when the gel is autoclaved for 20 hr (Fig. 4). No ZSM-23 crystals are formed after autoclave times of 20 hr. When the autoclave time is increased, the pH is accordingly increased. These data may suggest that hydroxyl groups are initially formed as intermediates prior to crystallization of ZSM-23 zeolites. This yields a decrease in pH at a short autoclave time (<20 hr). After the intermediates are converted to crystalline ZSM-23 zeolites, hydroxyl groups are then released into the solution. Therefore, the pH for the mother liquors is increased as autoclave time exceeds 20 hr.

X-ray diffraction patterns (Fig. 2) confirm that the prepared materials have the ZSM-23 structure. ZSM-23 zeolites have been assigned to the MTT framework. (22) Lattice parameters of a = 5.01 Å, b = 23.52 Å, and c = 11.13 Å are calculated from such XRD patterns. XRD data (Fig. 3) also suggest that the longer the autoclave time, the more crystalline the materials. This suggestion is also supported by FT-IR studies (Figs. 6a and 6c). Both hydroxyl groups of terminal silanol and acid sites are observed at 3744 and 3609 cm^{-1}, respectively. The ratio of hydroxyl group of terminal silanol to that of acid sites decreases from 4.25 to 0.92 for samples autoclaved for

40 and 100 hr, respectively. The fewer hydroxyl groups of terminal silanol the material contains, the better the crystallinity of the material. Therefore, as the autoclave time increases, the crystallinity of the materials increases.

Greater crystallinity of ZSM-23 materials leads to more Brønsted acid sites than Lewis acid sites, which is supported by studies of pyridine chemisorption (Figs. 6b and 6d). When the autoclave time is increased from 40 to 100 hr, the ratio of Brønsted acid sites to Lewis acid sites is increased from 1.50 to 7.58. Brønsted acid sites are created by hydroxyl groups which are bridged between framework aluminum and silicon ions. Lewis acid sites are originated from terminal aluminum ions which contain empty *p* orbitals. Therefore, more crystalline ZSM-23 materials lead to more bridged hydroxyl groups (Brønsted) and fewer terminal aluminum ions (Lewis).

More crystalline ZSM-23 materials also have less volume of mesopores (10–100 Å), as concluded from comparison of data of pore size distributions for ZSM-23 zeolites autoclaved for 40 and 100 hr as shown in Table 1. Therefore, ZSM-23 zeolite autoclaved for 100 hr has a smaller surface area of meso-/macropores (198 m^2/g) than that autoclaved for 40 hr (278 m^2/g).

Theoretically, more crystalline materials should have more volume of micropores (<10 Å). However, experimental data in Table 1 show that ZSM-23 zeolite autoclaved for 100 hr has a smaller volume of micropores (58.4 $\mu l/g$) than that autoclaved for 40 hr (69.2 $\mu l/g$). The reason for contradiction between theoretical expectations and experimental results relates to the fact that adsorption data of nitrogen molecules were used to determine the micropore distributions. The nitrogen molecule itself has a radius of 4.54 Å. However, ZSM-23 zeolites contain one-dimensional channels of 10-member rings (4.5 × 5.2 Å). Hence, experimental data from nitrogen adsorption have their limitations as probes of micropores which are smaller than or similar to the size of nitrogen molecules.

However, results of micropore distributions determined by nitrogen adsorption are still useful for interpretation of microporous properties of different crystalline materials. ZSM-23 zeolite materials of poor crystallinity contain more shorter-distance channels of 4.5 × 5.2 Å. Obviously, it would have more pore mouths of 4.5 × 5.2 Å channels. These kinds of pore mouths actually show greater diameters than 4.5 × 5.2 Å in the experiment of pore size distributions. Micropore distributions of ZSM-23 zeolite autoclaved for 40 hr as illustrated in Fig. 5a show that the maximum distribution of micropores is located at about 5.7 Å. As autoclave time is increased to 100 hr, ZSM-23 zeolite becomes more crystalline. The length of zeolite channels of 4.5 × 5.2 Å is accordingly increased. Amounts of pore mouths of 4.5 × 5.2 Å channels are then decreased. Therefore, the micropore distributions for ZSM-23 zeolites (Fig. 5b) are decreased by about a factor of 2. At the same time, the pore size of the distribution maximum is shifted from 5.7 to 5.2 Å.

B. Adsorptive Shape Selectivity

Zeolite ZSM-23 is a shape selective material for adsorption of but-1-ene and isobutylene molecules, as suggested by temperature-programmed desorption data for ammonia, but-1-ene, and isobutylene. Ammonia is normally used to probe the acidity of ZSM-23 zeolites. The strength of acid sites is determined by the desorption temperature. The higher the desorption temperature, the stronger the interaction between ammonia and acid sites. The amount of acid sites can be determined by the amount of desorbed ammonia which is calculated from the peak area after peak calibration with a known-volume sample loop. Ammonia TPD data (Fig. 7a) suggest that there are two types of acid sites (weak and strong) in the fresh ZSM-23 zeolites. Both weak and strong acid sites in ZSM-23 zeolites are available for but-1-ene molecules (Fig. 8a). However, isobutylene, a more bulky molecule, can only access about 42% of the acid sites (Fig. 9a).

Zeolite ZSM-23 becomes more shape selective for adsorption of but-1-ene and isobutylene after this material is treated with but-1-ene. Adsorption studies of ammonia, but-1-ene, and isobutylene on the used ZSM-23 zeolites (Figs. 7b, 8b, and 9b, respectively) support this suggestion. After ZSM-23 zeolites are used as catalysts for *n*-butene skeletal isomerization for 20 hr time on stream, about 35% of the strong acid sites or 16% of total acid sites are poisoned by coke. There is no loss of weak acid sites. The broadening of the ammonia desorption peak at low temperature implies that the diffusion of ammonia inside zeolite channels is more difficult for used catalysts than fresh ones. Such slow diffusion of ammonia may also be due to coke formation inside zeolite channels. However, catalytic reactions on ZSM-23 zeolite for 20 hr reduce the amount of acid sites (available for but-1-ene) by 87% as compared to that for fresh ZSM-23 zeolite. For these reduced acid sites which react with butene, 16% are due to poisoning of acid sites by the deposited coke, and 71% are due to partial blocking of zeolite channels. The amount of acid sites (13%) probed by but-1-ene is the same as that probed by isobutylene.

Partial blocking of zeolite channels by coke formation is illustrated in Fig. 5. The fresh catalyst (ZSM-23 zeolite autoclaved for 100 hr) has a distribution of micropores centered at about 5.2 Å (Fig. 5b). However, these micropores are blocked by deposited coke to a size which can not be probed by nitrogen molecules (Fig. 5c). Such partial blocking of zeolite channels prevents 71% of the acid sites from interaction with but-1-ene molecules. It also reduces the space around acid sites so as to achieve high selectivity for *n*-butene skeletal isomerization, instead of dimerization of butene molecules.

C. Catalysis

Zeolite ZSM-23 is a shape-selective catalyst for skeletal isomerization of *n*-butene to isobutylene at 733 K with extremely high space velocities of but-1-ene (170.88 to 341.76 WHSV) (Figs. 10 and 11). For such high space velocities, zeolite ZSM-23 is still very stable as regards yields and selectivities to isobutylene. Therefore, average values for the conversions of *n*-butene, yields of isobutylene, and selectivities to isobutylene are used for discussion. By increasing the space velocity of but-1-ene from 170.88 to 341.76 WHSV, the yield of isobutylene is decreased from 28.17 to 19.85% and the selectivity to isobutylene is increased from 84.80 to 91.93%. Based on these kinetic data, it is estimated that about 1.31 but-1-ene reactant molecules are converted to their products per second on each aluminum site for a space velocity of but-1-ene of 341.76 WHSV. Furthermore, such a large span of but-1-ene space velocity might allow great flexibility for process operation. Such high space velocities of reactants may significantly reduce the size of industrial reactors. The stability of these systems might simplify process operation and lower operation costs.

In addition, pentenes account for about one half of the side products in the process of *n*-butene skeletal isomerization. More than 85% of these pentenes are isopentenes which are raw materials for the production of *t*-amyl methyl ether (TAME), another excellent oxygenate which can be used to boost gasoline octane number. Therefore, selectivity to isoolefins is even higher if isopentenes are also taken into consideration.

Of the four butene isomers, isobutylene is predicted to form at about 38.4% at 733 K and 40.4% at 693 K based on thermodynamic calculations. At 693 K, the conversion of *n*-butene is decreased from 80.74 to 45.17% and selectivity to isobutylene is increased from 21.37 to 64.65% with increasing but-1-ene space velocity from 5.34 to 85.44 WHSV (Table 2). Maximum yields of isobutylene (31.91%) occur at a but-1-ene space velocity of 42.72 WHSV. These data suggest that the longer contact time (the smaller space velocity) favors side reactions such as secondary and tertiary reactions.

Reaction temperature is further decreased from 693 to 653 K at a but-1-ene space velocity of 80.44 WHSV. Accordingly, isobutylene yield is decreased from 29.13 to 21.61% (Table 2). However, side products are increased from 16.04 to 17.75%. Hence, the selectivity to isobutylene is decreased from 64.65 to 54.95%. These data suggest that the activation energy for *n*-butene isomerization is higher than that for side reactions such as dimerization of butene molecules. Therefore, increasing reaction temperature accelerates skeletal isomerization more than dimerization reactions.

Since only olefins containing up to eight carbon atoms were observed in the product stream, dimerization of butene molecules is believed to be a primary side reaction for *n*-butene skeletal isomerization. Such dimers are then cracked to form propylene and pentenes via β-scission of carbenium ion intermediates (secondary reaction). Propylene molecules are dimerized to form hexenes (tertiary reaction). Codimerization of propylene and butene molecules leads to formation of heptenes (tertiary reaction). A proposed reaction mechanism for formation of side products is mainly deduced from the following two facts (1) *n*-butane formation is a primary reaction (hydrogenation of *n*-butene), and (2) isobutane formation is a secondary reaction (conversion of *n*-butene to isobutylene is followed by hydrogenation of isobutylene). The source of hydrogen for *n*-butane/isobutane formation is referred to as hydrogen transfer during formation of aromatics. Increasing the but-1-ene space velocity would yield a decrease in contact time. Both *n*-butane and isobutane formation should be decreased as the contact time decreases (the space velocity of but-1-ene increases). However, a decrease of isobutane formation should be faster than for *n*-butane formation. Figure 12 confirms this deduction that the ratio of isobutane to *n*-butane is decreased with but-1-ene space velocity.

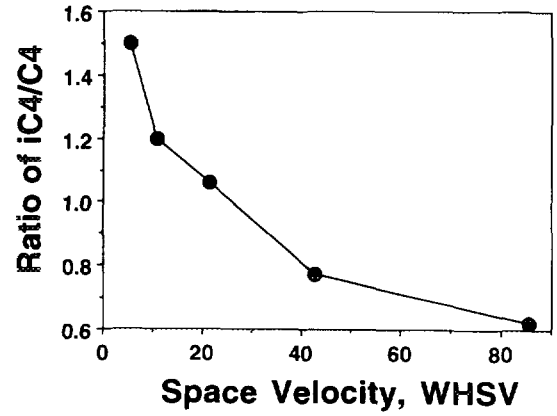

FIG. 12. Correlation of the ratio of isobutane to *n*-butane with space velocity of *but*-1-ene.

Based on the above proposed mechanism, pentenes are the products of secondary reactions, while hexenes and heptenes are the products of tertiary reactions. Ratios of hexenes and heptenes to pentenes are plotted with but-1-ene space velocity in Fig. 13. Both curves show decreasing trends with an increase in but-1-ene space velocity (a decrease in contact time). In fact, the concentration of propylene always decreases with but-1-ene space velocity, while the concentration of *n*-butene increases with but-1-ene space velocity. The higher the concentration of butene, the faster the product formation from butene reactants. Therefore, effects of reactant concentrations

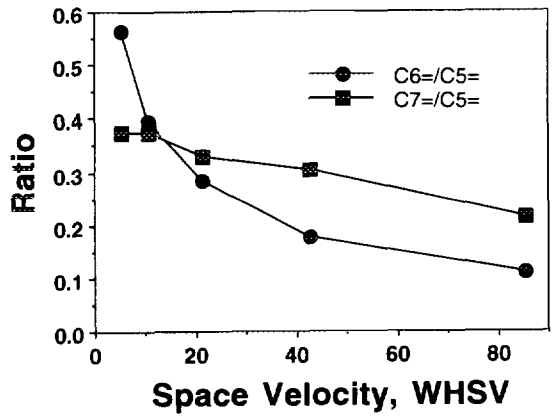

FIG. 13. Correlation of ratios of hexenes to pentenes (circle) and heptenes to pentenes (square) with space velocity of *but*-1-ene.

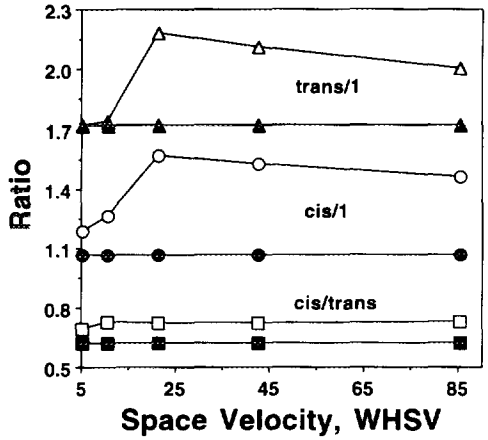

FIG. 14. Comparison of thermodynamic (solid marks) and experimental (open marks) ratios of *n*-butene isomers. (triangle, *trans-but*-2-ene to but-1-ene; circle, *cis-but*-2-ene to *but*-1-ene; square, *cis-but*-2-ene to *trans*-but-2-ene).

have a profound influence on the ratio of hexenes to pentenes and that of heptenes to pentenes. All these results suggest that the formation of hexenes and heptenes is a subsequent reaction step as compared to the formation of pentenes. Hexenes are formed by the dimerization of propylene molecules, and heptenes are formed by the codimerization of propylene and butene molecules. The above proposed mechanism is based on the assumption that octenes are the products of primary reactions and the reactants in secondary reactions. This assumption is supported by the fact that there is a maximum in formation of octenes (4.18%) at a but-1-ene space velocity of 42.72 WHSV.

The distribution of the three *n*-butene isomers does not follow thermodynamic equilibrium. The thermodynamic data for four isomers of butene were calculated by using changes of Gibbs free energy in Ref. (23). Thermodynamic ratios of *trans*-but-2-ene to but-1-ene, *cis*-but-2-ene to but-1-ene, and *cis*-but-2-ene to *trans*-but-2-ene at 693 K are 1.72, 1.06, and 0.618, respectively. Figure 14 shows experimental data (open marks) and thermodynamic data (solid marks) for *trans*-but-2-ene to but-1-ene (triangle) and *cis*-but-2-ene to but-1-ene (circle) ratios. Experimental data for these two ratios are greater than their thermodynamic equilibrium data. This implies that but-1-ene molecules are overconverted to *trans*- and *cis*-but-2-enes.

Furthermore, the ratio of *cis*-but-2-ene to *trans*-but-2-ene (open square) is greater than thermodynamic data (solid square), as also shown in Fig. 14. At low temperature (below or around room temperature) and at early times on stream for but-1-ene double bond migration, *cis*-but-2-ene is an exclusive product for catalysts of small pore zeolites, such as ferrierite (24), NU-10 (25), and EU-12 (26).

Leach and co-workers (24–26) have proposed a mechanism to describe such preferential formation of *cis*-but-2-ene. Double bond migration of but-1-ene over acid catalysts is generally considered to occur via secondary butyl carbenium ions. In small pore zeolites there are steric interactions between pore walls and the methyl group of the secondary butyl carbenium ions. Therefore, the rotation of the C_2^+–C_3 bond in this carbenium ion is greatly restricted by such steric interactions between the methyl group and the pore wall. H^+ abstraction from the C_3 atom of the secondary butyl carbenium can occur in two ways. One way for H^+ abstraction requires a methyl group rotation for formation of *trans*-but-2-ene, while the other way leads to formation of *cis*-but-2-ene without rotating the methyl group. For medium pore zeolites ZSM-5 and ZSM-11, the three *n*-butene isomers reach their thermodynamic equilibrium (24). Steric constraints between the pore wall of medium pore zeolites and the methyl group of the secondary butyl carbenium ion are removed as compared to the small pore zeolite, ZSM-23.

Finally, isobutylene reacts over zeolite ZSM-23 with conversions of isobutylene and selectivities to *n*-butene which are similar to those for but-1-ene as a feed, as shown in Table 2. The distribution of side products for both feed systems is also very similar except for *n*-butane and isobutane. This suggests that formation of isobutylene from *n*-butene via the methyl cyclopropane carbenium ion is a reversible process. The formation of side products is due to both *n*-butene and isobutylene reactants. In addition, isobutylene as a feed for zeolite ZSM-23 produces more isobutane (0.59%) than *n*-butane (0.18%). However, but-1-ene as a feed for ZSM-23 produces less isobutane (0.48%) than *n*-butane (0.77%). These data also suggest that formation of *n*-butane is a primary side reaction and formation of isobutane is

a secondary side reaction in *n*-butene skeletal isomerization to isobutylene.

CONCLUSIONS

Zeolite ZSM-23 has been prepared with hydrothermal methods by using pyrrolidine as a structure-direct template. This zeolite has rice shape morphology, consistent with literature results. Zeolite ZSM-23 contains one-dimensional channels of 4.5 × 5.2 Å and it is shape selective for adsorption of ammonia, but-1-ene, and isobutylene molecules. The used ZSM-23 catalysts are more shape selective for adsorption of but-1-ene and isobutylene due to coke deposition.

n-Butene can be selectively isomerized to isobutylene on zeolite ZSM-23 with 20 to 30% yields of isobutylene. Extremely high space velocities of but-1-ene, good stability and activity, and large viable variations in but-1-ene space velocities are characteristic of ZSM-23 zeolites for such catalytic systems.

Formation of isobutylene from *n*-butene via methyl cyclopropane carbenium ion intermediates is a reversible process. Dimerization of butene molecules is a primary side reaction which accompanies *n*-butene skeletal isomerization. Octenes (products of primary reactions) are further cracked into propylene and pentenes via β-scission of carbenium intermediates (secondary reaction). Formation of hexenes and heptenes is a tertiary reaction which occurs by dimerization of propylene and codimerization of propylene and butene molecules, respectively. Small amounts of light alkanes are also formed via hydrogen transfer from the formation of aromatics. Distributions of the three *n*-butene isomers show that but-1-ene is overconverted to *cis*-but-2-ene and *trans*-but-2-ene. The perferential formation of *cis*-but-2-ene is due to a strong steric interaction between the pore wall of small pore ZSM-23 zeolites and methyl groups of secondary carbenium ions.

ACKNOWLEDGMENT

The authors thank the Office of Basic Energy Sciences, Division of Chemical Sciences, Department of Energy and Texaco, Inc. for supporting this research.

REFERENCES

1. Pecci, G., and Floris, T., *Hydrocarbon Process.* **56,** 98 (1977).
2. Szabo, J., Perrotey, J., Szabo, G., Duchet, J. C., and Cornet, D., *J. Mol. Catal.* **67,** 79 (1991).
3. Choudhary, V. R., *Chem. Ind. Dev.* 32 (1974).
4. Wojciechowski, B. W., and Corma, A., "Catalytic Cracking: Catalysis, Chemistry and Kinetics," p. 100. Dekker, New York, 1986.
5. Thomas, J. M., *Sci. Am.* **Apr.,** 112 (1992).
6. Harandi, M. N., Owen, O., and Mead, B., U.S. Patent 5,024,679 (1991).
7. Xu, W.-Q., Suib, S. L., and O'Young, C.-L., *J. Catal.* **144,** 285 (1993).
8. Simon, M. W., Nam, S. S., Xu, W.-Q., Suib, S. L., Edwards, J. C., and O'Young, C.-L., *J. Phys. Chem.* **96,** 6381 (1992).
9. Simon, M. W., Xu, W.-Q., Suib, S. L., and O'Young, C.-L. *Microporous Mater.* **2,** 477 (1994).
10. Bianchi, D., Simon, M. W., Nam, S. S., Xu, W.-Q., Suib, S. L., and O'Young, C.-L., *J. Catal.* **145,** 551 (1994).
11. Grandvallet, P., de Jong, K. P., Mooiweer, H. H., Kortbeek, A. G. T., and Kraushaar-Czarnetzki, B., European Patent 501, 577 (1992).
12. Powers, D. H., Murray, B. D., Winquist, B. H. C., Callender, E. M., and Varner, J. H., European Patent 523,838 (1993).
13. Xu, W.-Q., Yin, Y.-G., Suib, S. L., and O'Young, C.-L., submitted for publication.
14. Wright, P. A., Thomas, J. M., Millward, G. R., Ramdas, S., and Barri, S. A., *J. Chem. Soc., Chem. Commun.*, 1117 (1985).
15. Horvath, G., and Kawazoe, K., *J. Chem. Eng. Jpn.* **15,** 470 (1983).
16. Xu, W.-Q., and Suib, S. L., *J. Catal.* **145,** 65 (1994).
17. Messner, A. E., Rosie, D. M., and Argabright, P. A., *Anal. Chem.* **31,** 230 (1959).
18. Rosie, D. M., *Anal. Chem.* **29,** 1263 (1957).
19. Ernst, S., Kumar R., and Weitkamp, J., *in* "Zeolite Synthesis" (M. L. Occelli, H. E. Robsons, Eds.), *ACS Symp. Ser.*, Vol. 398, p. 560. Maple Press, Los Angeles, 1989.
20. Kumar, R., Thangaraj, A., and Rajmohanan, P., *Indian J. Chem., Sect. A* **29A,** 1083 (1990).
21. Kumar, R., and Ratnasamy, P., *J. Catal.* **121,** 89 (1990).
22. Rohrman, A. C., Jr., LaPierre, R. B., Schlenker, J. L., Wood, J. D., Valyocsik, E. W., Rubin, M. K., Higgins, J. B., and Rohrbaugh, W. J., *Zeolites* **5,** 352 (1985).
23. Rossini, F. D., Pitzer, K. S., Arnett, R. L., Braun, R. M., and Pimentel, G. C., "Selected Values of Physical and Thermodynamic Properties of Hydrocarbons and Related Compounds." The American Petroleum Institute, Project 44, Carnegie Press, Pittsburgh, 1953.
24. Harrison, I. D., Leach, H.F., and Whan, D. A., *Zeolites* **7,** 21 (1987).
25. Harrison, I. D., Leach, H. F., and Whan, D. A., *Zeolites* **7,** 28 (1987).
26. Araya, A., Blake, A. J., Harrison, I. D., Leach, H. F., Lowe, B. M., and Whan, D. A., *Zeolites* **12,** 24 (1992).